JOURNAL OF GEOPHYSICAL RESEARCH, VOL. 113, B04307, doi:10.1029/2007JB005166, 2008



# Crustal structure and apparent tectonic underplating from receiver function analysis in South Island, New Zealand

Sonja Spasojević[1] and Robert W. Clayton[1]

Received 11 May 2007; revised 3 October 2007; accepted 24 November 2007; published 24 April 2008.

[1] We utilize seismic converted phases on more than 700 receiver functions calculated for 42 stations in the South Island, New Zealand, to infer crustal and uppermost mantle structure. We determine the crustal thickness from direct observations of conversion from the Moho interface and infer zone of the maximum thickness being located along the axis of the Southern Alps, just east from the Alpine fault. The crustal root widens from north to south in the direction perpendicular to the Alpine fault and appears to have an asymmetric structure. Stations in the alpine portion of island show evidence for prominent midcrustal conversions. Significant crustal thickening is developed in response to both the convergent component of the motion on the Alpine fault and subduction in the Fiordland region. We propose two models for a strong uppermost mantle conversion that occurs at depths between 33 and 83 km on 16 stations and forms a large continuous feature along the east coast and in the central portions of the South Island. Our preferred model attributes upper mantle conversion to tectonically underplated oceanic crust formed by late Oligocene-Miocene spreading between the Australian and Pacific plates, which was detached from the Australian plate and tectonically underplated under the South Island. An alternative model attributes the upper mantle conversions to long-lived seismic fabric created by subduction of the Gondwanaland margin.

**Citation:** Spasojević, S., and R. W. Clayton (2008), Crustal structure and apparent tectonic underplating from receiver function analysis in South Island, New Zealand, *J. Geophys. Res.*, *113*, B04307, doi:10.1029/2007JB005166.

## 1. Introduction

[2] The South Island, New Zealand straddles the Pacific and Australian plates (Figure 1). At present, the Pacific plate is subducting under the Australian plate at the Hikurangi Trough in the northern South Island (Figure 1), and the Australian plate is subducting under the Pacific plate in the southwest at the Puysegur Trench and Fiordland Trough. The oblique dextral strike-slip Alpine fault crosses almost the entire South Island (Figure 1), and it accommodates approximately 50–70% of the total present-day plate motion [*Sutherland et al.*, 2000]. The Pacific and Australian plates are converging obliquely in this region, resulting in a significant lithospheric thickening that is developed in a response to the shortening [*Walcott*, 1998]. The total relative motion between the Australian and Pacific plates is 39–46 mm/a, and it can be separated into 37–40 mm/a of strike-slip motion parallel to the Alpine fault, and 11–22 mm/a of convergent motion normal to the Alpine fault in the central South Island [*Walcott*, 1998; *Norris et al.*, 1990]. The convergence resulted in the uplift of the Southern Alps, with current uplift rates being 5–10 mm/a [*Norris et al.*, 1990].

[3] The South Island is a region with an active young orogeny, where models of convergent mountain belts can be readily tested with geophysical observations. Studies of the lithospheric structure can provide important information about mechanisms that control uplift, lithospheric deformation, and associated mantle flow, providing more insights in the behavior of continental lithosphere under compression. Crustal structure of the South Island has been previously explored, especially since an extensive set of geophysical experiments was conducted in 1995–96. It included an active source reflection-refraction seismic experiment SIGHT (South Island Geophysical Transect), a passive seismology experiment SAPSE (Southern Alps Passive Source Experiment), magnetotelluric and electrical studies. Detailed two-dimensional lithospheric structure has been defined along the SIGHT transects in the central portion of the South Island, indicating that the crustal root is approximately 100 km wide, with the crust having a maximum thickness of 37 to 44 km [*Scherwath et al.*, 2003; *Van Avendonk et al.*, 2004] along the main SIGHT transects 1 and 2, respectively. *Van Avendonk et al.* [2004] calculate, based on the two-dimensional (2-D) crustal structure obtained along transect 2, that total amount of crustal shortening is around 80–100 km. *Henrys et al.* [2004] define a partial 3-D image of the Moho in the central portions of the South Island using seismic reflections, and find a pronounced crustal root approximately 80 km wide, with maximum Moho depth of 45 km on transect 2. Local

[1]Seismological Laboratory, California Institute of Technology, Pasadena, California, USA.


0148-0227/08/2007JB005166$09.00

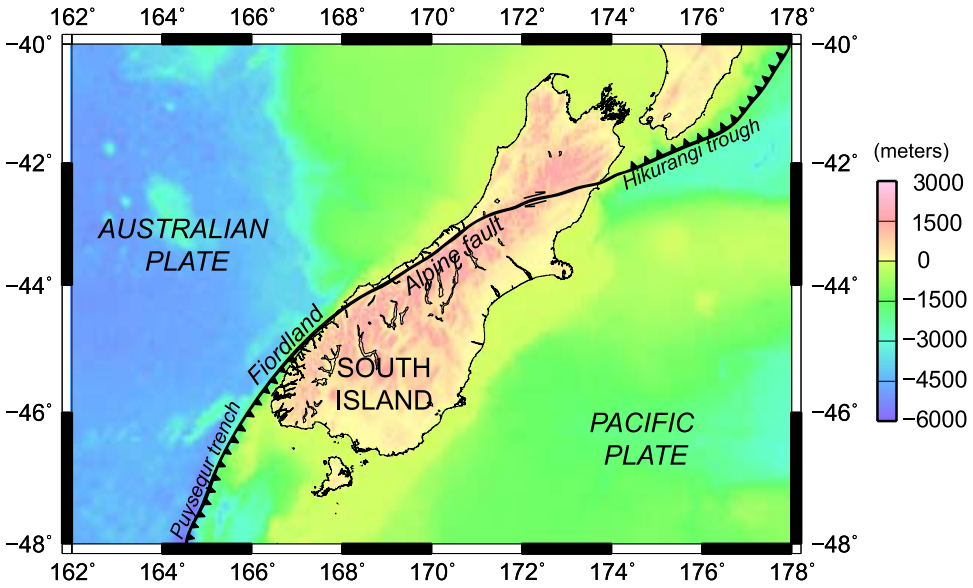


**Figure 1.** Tectonic setting of the South Island, New Zealand, shown on the bathymetry map. The Pacific plate is subducting under the Australian plate at the Hikurangi trough; the Australian plate is subducting under the Pacific plate at the Puysegur trench and in the Fiordland. The oblique dextral strike-slip Alpine fault marks the plate boundary in the largest portion of the South Island.

three-dimensional lithospheric velocity models are developed for subduction regions of Fiordland [*Eberhart-Phillips and Reyners*, 2001] and Hikurangi [*Eberhart-Phillips and Reyners*, 1997]. Three-dimensional studies for the whole South Island utilized mostly traveltime tomographic inversion [*Kohler and Eberhart-Phillips*, 2002; *Eberhart-Phillips and Bannister*, 2002] to define the deepest Moho below the axis of the Southern Alps, some 40 km east of the Alpine fault.

[4] In this paper we present a three-dimensional model of crustal thickness observed on an extensive set of more than 700 receiver functions calculated for 42 stations in permanent New Zealand National Seismic Network (NZNSN) and temporary SAPSE network. This model is based on a direct observation and mapping of P-to-S conversion from Moho interface, and as such represents an extension of previous 2-D and partial 3-D models, such as ones presented by *Scherwath et al.* [2003], *Van Avendonk et al.* [2004], *Henrys et al.* [2004], and *Godfrey et al.* [2001]. It provides important additional constraints on the 3-D crustal structure of the South Island, since previous full 3-D models were defined using traveltime tomography and utilizing first arrivals only [e.g., *Kohler and Eberhart-Phillips*, 2002; *Eberhart-Phillips and Bannister*, 2002] and were not necessarily based on direct observations of velocity discontinuities, but rather definition of Moho interface from an isovelocity surface.

[5] We also explore strong uppermost mantle P-to-S conversions observed on many receiver functions calculated in the region of the South Island, and offer models that could potentially explain plate tectonic association of this conversion. Cretaceous-Cenozoic tectonics is primarily responsible for the present shape of New Zealand [*Sutherland*, 1999]. In the period between 130 and 80 Ma, there was a change from subduction to extension that resulted in the formation of the Tasman Sea and South Pacific [*Sutherland*, 1999]. New Zealand was a passive margin in period between late Cretaceous and late Eocene [*Sutherland*, 1999], with not much tectonic activity. The plate boundary between the Australian and Pacific plates in the South Island formed progressively in the last 45 Ma [*Sutherland et al.*, 2000]. The passive Eocene margin separated the Paleozoic Challenger plateau and significantly younger oceanic lithosphere and it structurally controlled position of the Alpine fault [*Sutherland et al.*, 2000]. Oblique strike-slip motion since 25 Ma along the Alpine fault translated the passive margin into the continental collision zone, causing subduction of the oceanic lithosphere and localization of the shear strain near the Alpine fault [*Sutherland et al.*, 2000]. Initially minor Miocene compression increased significantly around 6 Ma, as a result of a change of position of the Australian-Pacific pole of motion to the west-southwest [*Walcott*, 1998; *Cande and Stock*, 2004a], resulting in the uplift of the Southern Alps. A total of approximately 100 km of shortening occurred in the South Island, New Zealand [*Walcott*, 1998]. A significant amount of crust in the region of the South Island is unaccounted for based on different models of the plate motions and different tectonic reconstructions [*Cande and Stock*, 2004a; *Sutherland et al.*, 2000]. We investigate the potential association of the uppermost mantle conversion features with this crust, potentially providing new contributions on the understanding of the plate motions and geodynamics in the region.

## 2. Methodology

### 2.1. Receiver Functions Theory

[6] Receiver function analysis is a technique to map the subsurface structure beneath the seismic stations by enhanc-

ing converted phases. Three-component seismic recording $X$ in the time domain due to a teleseismic P wave can be written as [*Langston*, 1979]

$$X_V(t) = I(t)*S(t)*E_V(t) \quad (1)$$

$$X_R(t) = I(t)*S(t)*E_R(t) \quad (2)$$

$$X_T(t) = I(t)*S(t)*E_T(t) \quad (3)$$

where *I(t)* is the impulse recording instrument response, *S(t)* is the seismic source function, *E(t)* is the impulse response of the near-receiver Earth's structure. Subscripts *V*, *R*, *T* indicate vertical, radial and transverse components, respectively, and asterisk denotes convolution.

[7] *Langston* [1979] showed that $E_V(t)$ is an approximate delta function $\delta(t)$, under the assumption that very little converted energy appears on the vertical component for near vertical rays. Therefore, we can use $X_V(t)$ to deconvolve the instrument response *I(t)* and the seismic source function *S(t)* from the radial and transverse component recordings, and effectively define Earth's structure under the seismic station. The radial $f_R$ and transverse $f_T$ receiver functions can be calculated by deconvolution in the frequency domain [*Parker*, 1999]:

$$f_R = \frac{X_R(f)X_V^*(f)}{X_V(f)X_V^*(f) + \sigma^2} F_G(f) \quad (4)$$

$$f_T = \frac{X_T(f)X_V^*(f)}{X_V(f)X_V^*(f) + \sigma^2} F_G(f) \quad (5)$$

where *Xv*, *Xr* and $X_T$ are the vertical, radial and transverse seismograms respectively, $\sigma$ is a parameter used to stabilize the deconvolution process, $X_V^*(f)$, symbolizes complex conjugate of $X_V(f)$, and $F_G(f)$ is Gaussian-shaped filter applied in the frequency domain to smooth the receiver function.

[8] We implement the stacking algorithm of *Zhu and Kanamori* [2000] which utilizes both primary P-to-S converted phase and multiple phases PpPs and PpSs + PsPs to determine crustal thickness and the $V_p/V_S$ ratio ($\kappa$ parameter). When only primary P-to-S converted phase is used, there is a strong trade off between crustal thickness and the Vp/Vs ratio, which can be significantly reduced when both primary converted and multiple phases are used [*Zhu and Kanamori*, 2000].

[9] Crustal thickness estimate H using time separation $t_{Ps}$ between Ps and P arrivals is given as [*Zhu and Kanamori*, 2000]

$$H = \frac{t_{Ps}}{\sqrt{\frac{1}{v_S^2} - p^2} - \sqrt{\frac{1}{v_P^2} - p^2}} \quad (6)$$

where $p$ is the ray parameter, and $V_P$ and $V_S$ represent average P and S wave crustal velocities, respectively. There is a strong trade-off between estimated crustal thickness and crustal velocity, and especially estimated crustal thickness and the $\kappa$ parameter. *Zhu and Kanamori* [2000] show that for average $V_P$ = 6.3 km/s, $\kappa$ = 1.732 and H = 30 km, uncertainty in determining crustal thickness can be expressed as

$$\Delta H = \frac{\delta H}{\delta V_P}\Delta V_P = 4.3\Delta V_P \quad (7)$$

$$\Delta H = \frac{\delta H}{\delta \kappa}\Delta \kappa = -40.2\Delta \kappa \quad (8)$$

Crustal thickness estimate has relatively stronger dependence on $\kappa$ parameter than on Vp. For example, change in Vp of 0.1 km/s introduces less than 0.5 km change in H, and similar depth error is introduced by change of $\kappa$ parameter of 0.01. Estimates of the average crustal Vp in the South Island vary by approximately 0.4 km/s [*Melhuish et al.*, 2005; *Scherwath et al.*, 2003; *Van Avendonk et al.*, 2004; *Davey et al.*, 1998], and using equation (7) this leads to a depth uncertainty of approximately ±2 km. This inherent ambiguity can be significantly reduced when crustal multiples $P_PP_S$ and $P_PS_S + P_SP_S$ are used along with primary phases [*Zhu and Kanamori*, 2000].

[10] The stacking algorithm sums the amplitudes of receiver function at predicted arrival times of multiple phases for different values of crustal thickness and Vp/Vs ratios. The best estimates of crustal thickness and Vp/Vs ratios are found by scanning over a range of the two parameters and picking the set that maximizes the stacked amplitude. The procedure requires locally flat interfaces beneath the station to work effectively. We will refer to this procedure as the H-Vp/Vs method in this paper. More details on the procedure used for calculating receiver functions and the determination of crustal thicknesses using receiver functions are given by *Langston* [1979] and *Zhu and Kanamori* [2000].

### 2.2. Data Description

[11] We used 92 teleseismic events (Table S1 in the auxiliary material[1]) with epicentral distances between 25 and 100 degrees to calculate receiver functions. Forty-eight events with magnitude range 6.3–8.2 occurred in the period between November 1995 and December 1996 (Table S1), and were recorded on stations in the temporary SAPSE network. The remaining 44 events with magnitudes between 6.5 and 9 occurred in the 4 year period between 2003 and 2006, and were recorded on stations in permanent NZNSN network (Table S1). The azimuthal distribution of the events used in this paper is not optimal (Figure 2) since most of the events originated to the northwest and north. This results in a bias of the stacked receiver functions toward the structure to the northwest and north of the station. However, this bias is limited to structure within approximately 15 km of the station for the crust and within 30 km of the station for the upper mantle.

[12] We calculated total of 736 receiver functions for 42 stations in the South Island. Twenty two stations were

[1] Auxiliary materials are available in the HTML. doi:10.1029/2007JB005166.

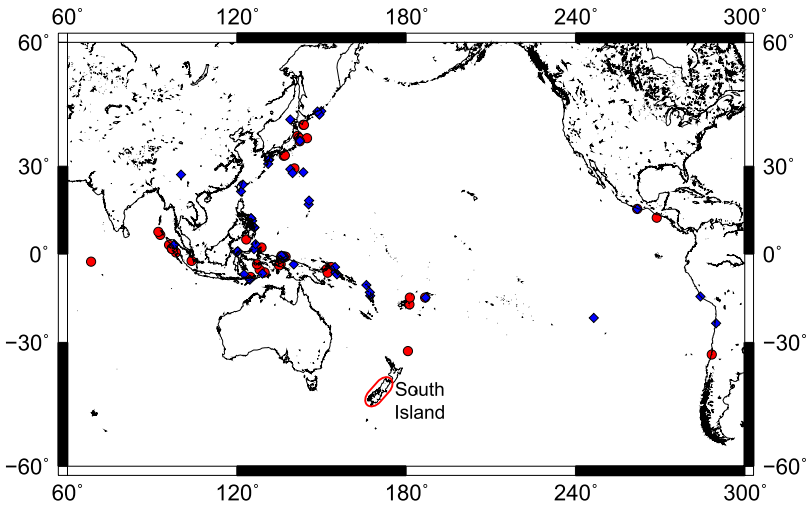


**Figure 2.** Distribution of teleseismic events used for calculation of receiver functions. Blue diamonds show events with magnitude 6.3 and higher recorded in the period 1995–1996 on SAPSE network, and red dots show events with magnitude 6.5 and higher recorded in the period 2003–2006 on NZNSN. We used events with epicentral distances between 25° and 100°.

operating in the period 1995/96 in the SAPSE network and twenty stations in the period 2003–2006 in the NZNSN network (Table 1) in the region of the South Island. Depending on the length of operation of a seismic station, seismic network, and the quality of seismic recording, the number of receiver function per station varies between 1 and 40 (Table 1). The network of seismic stations is not distributed uniformly throughout the South Island (Figure 3) and it is the densest in the central portion of the island, and sparsest in the south and north.

[13] We also attempted to calculate receiver functions for 21 three-component locations along the main SIGHT transect 1. The temporary SIGHT network was operating continuously during two periods in February 1996, and several teleseismic events were recorded. However, the receiver functions for nine teleseismic events with magnitude 6.0 and higher were of very poor quality, due to the high-frequency sensors (4 Hz).

### 2.3. Procedure for Calculation of Receiver Functions

[14] We calculate both radial and transverse receiver functions using approach described with equations (4) and (5), after applying a series of preprocessing steps. We select a time window of 90 s for all records, starting 15 s before P wave onset. A band-pass filter 0.02–2Hz was applied to records before rotation of two horizontal components into the radial and horizontal directions. We use the frequency domain deconvolution, as described by equations (4) and (5), with water levels $\sigma$ 0.001, 0.01, and 0.1, and Gaussian filter parameters of 2.5 and 5.0. For each event-station pair, we calculate six different receiver functions using combination of above given water levels and Gaussian filter parameters, and then select the most representative receiver function. Presignal noise level is the most important factor that determines selection of water level and Gaussian parameters for each event-station pair. For receiver functions with sufficiently low presignal noise level, we select the lowest water level and higher Gaussian parameter. Higher presignal noise level usually requires selection of higher values of water level and smaller value of Gaussian filter.

[15] Once all receiver functions are calculated, we group them according to corresponding seismic station and apply the H-Vp/Vs method, using an average crustal velocity Vp = 6.3 km/s, and a search range Vp/Vs($\kappa$) = 1.65–1.85. Since we look for a number of interfaces, we modify the H-Vp/Vs method to estimate depth to interfaces in a number of ranges: (1) 20–60 km to define the strongest event that corresponds to the Moho discontinuity; (2) 10–25, 25–35, 35–45, and 45–55 km to precisely isolate and define crustal features and the Moho discontinuity; and (3) 45–80 km to further refine Moho and define upper mantle conversion features. For each of the depth ranges we established if receiver functions show evidence for existence of a strong conversion feature, predicted its multiples and determined the best depth and Vp/Vs ratio.

[16] Table 1 shows for each seismic station: P-Ps differential times and depths of interpreted crustal conversions, Moho discontinuity and upper mantle conversion; associated uncertainties in determining depths of each interface; determined Vp/Vs ($\kappa$) and its uncertainties. We primarily utilize the radial receiver functions for most of our analysis since they contain most of the converted seismic energy. Transverse receiver functions were only produced for the stations with a well-determined Moho depth.

## 3. Results and Discussion

### 3.1. Receiver Function Quality

[17] The receiver function quality (Table 1) has been assessed qualitatively for all seismic stations, using the following criteria: number of receiver functions per station; similarity and coherence of crustal and upper mantle conversion on the receiver functions for the same station and different events; and stability of the receiver function analysis. Stations that have less than 5 receiver functions, stations where conversion depths differ from event to event and do not stack coherently are categorized to have poor

**Table 1.** Information About Geographic Location of Stations, Receiver Function Quality and Features Mapped Using Radial Receiver Functions[a]

| Station code | Network | Longitude, deg | Latitude, deg | Number of Receiver Functions | Quality | Moho Conversion P-Ps Time, s | Moho Conversion P-Ps Depth, km | Uncertainty in Moho Depth, km | $\kappa$ (Vp/Vs) | Uncertainty in $\kappa$ (Vp/Vs) | Crustal Conversion P-Ps Time, s | Crustal Conversion P-Ps Depth, km | Uncertainty in Crustal Conversion Depth, km | Upper Mantle P-Ps Conversion Time, s | Upper Mantle P-Ps Conversion Depth, km | Uncertainty in Upper Mantle Conversion Depth, km |
|---|---|---|---|---|---|---|---|---|---|---|---|---|---|---|---|---|
| ARPA | SAPSE | 171.58 | −42.97 | 6 | Good | 6.77 | 56.0 | ±1.4 | 1.745 | ±0.031 | 2.79 | 22.3 | ±1.1 | - | - | - |
| BERA | SAPSE | 169.88 | −44.53 | 11 | Medium | 5.02 | 40.0 | ±1.0 | 1.773 | ±0.022 | 3.47 | 26.6 | ±1.4 | - | - | - |
| BLBA | SAPSE | 173.88 | −41.71 | 13 | Medium | - | - | - | - | - | - | 13.1 | ±1.8 | - | - | - |
| CHTA | SAPSE | 176.58 | −43.77 | 1 | Poor | - | - | - | - | - | - | - | - | - | - | - |
| CLAA | SAPSE | 170.04 | −45.79 | 8 | Medium | 2.68 | 21.3 | ±2.8 | 1.780 | ±0.055 | - | - | - | - | - | - |
| CLIA | SAPSE | 169.31 | −46.29 | 11 | Medium | 3.02 | 25.1 | ±1.4 | 1.743 | ±0.071 | - | - | - | 5.53 | 47.2 | ±2.1 |
| CRLZ | NZNSN | 172.62 | −43.58 | 35 | Good | 3.22 | 23.2 | ±0.5 | 1.830 | ±0.030 | - | - | - | 4.67 | 45.6 | ±2.2 |
| DCZ | NZNSN | 167.15 | −45.47 | 13 | Poor | - | - | - | - | - | - | - | - | - | - | - |
| DENA | SAPSE | 171.81 | −41.74 | 10 | Good | 4.12 | 30.3 | ±0.9 | 1.835 | ±0.035 | - | - | - | - | - | - |
| DSZ | NZNSN | 171.80 | −41.75 | 31 | Good | 3.84 | 30.2 | ±3.1 | 1.788 | ±0.088 | - | - | - | - | - | - |
| EAZ | NZNSN | 169.31 | −45.23 | 26 | Medium | - | - | - | - | - | - | - | - | - | - | - |
| EWZA | SAPSE | 170.85 | −43.51 | 12 | Good | 4.28 | 40.6 | ±2.1 | 1.655 | ±0.052 | - | - | - | 6.38 | 53.7 | ±1.7 |
| FOZ | NZNSN | 169.82 | −43.53 | 20 | Medium | - | - | - | - | - | - | - | - | - | - | - |
| GLAA | SAPSE | 169.85 | −43.42 | 4 | Medium | 3.88 | 29.5 | ±2.1 | 1.815 | ±0.060 | 1.98 | 15.4 | ±1.6 | - | - | - |
| GLEA | SAPSE | 168.41 | −44.87 | 1 | Poor | - | - | - | - | - | - | - | - | - | - | - |
| JACA | SAPSE | 168.61 | −43.97 | 2 | Medium | 3.74 | 32.7 | ±0.7 | 1.705 | ±0.030 | - | - | - | - | - | - |
| JCZ | NZNSN | 168.79 | −44.07 | 25 | Good | 4.29 | 32.0 | ±2.5 | 1.823 | ±0.083 | 2.48 | 18.5 | ±1.8 | - | - | - |
| KHZ | NZNSN | 173.54 | −42.42 | 39 | Good | 2.79 | 23.4 | ±1.7 | 1.733 | ±0.138 | - | - | - | 7.15 | 68.7 | ±3.2 |
| LAMA | SAPSE | 169.46 | −43.71 | 2 | Poor | - | - | - | - | - | - | - | - | - | - | - |
| LATA | SAPSE | 172.27 | −42.78 | 13 | Good | 4.34 | 31.9 | ±1.1 | 1.860 | ±0.037 | 1.97 | 17.3 | ±1.9 | 8.00 | 75.5 | ±1.9 |
| LBZ | NZNSN | 170.18 | −44.39 | 23 | Good | 3.47 | 29.9 | ±2.3 | 1.717 | ±0.083 | 1.75 | 14.4 | ±1.1 | 7.42 | 70.3 | ±2.7 |
| LTZ | NZNSN | 172.27 | −42.78 | 22 | Good | 4.40 | 32.4 | ±1.1 | 1.835 | ±0.042 | 2.04 | 16.6 | ±2.2 | 7.38 | 72.0 | ±2.2 |
| LU2A | SAPSE | 169.71 | −45.04 | 14 | Good | 3.68 | 30.1 | ±2.1 | 1.750 | ±0.072 | 2.26 | 21.7 | ±0.5 | - | - | - |
| MAKA | SAPSE | 169.22 | −44.25 | 8 | Medium | 4.25 | 40.3 | ±2.4 | 1.652 | ±0.057 | - | - | - | - | - | - |
| MAYA | SAPSE | 171.37 | −43.75 | 1 | Poor | - | - | - | - | - | - | - | - | - | - | - |
| MLZ | NZNSN | 168.12 | −45.37 | 28 | Medium | 5.37 | 45.4 | ±0.7 | 1.727 | ±0.019 | - | - | - | - | - | - |
| MQZ | NZNSN | 172.65 | −43.71 | 40 | Good | 2.98 | 25.0 | ±1.0 | 1.735 | ±0.040 | - | - | - | 8.31 | 82.7 | ±2.2 |
| MSZ | NZNSN | 167.93 | −44.68 | 11 | Poor | - | - | - | - | - | - | - | - | - | - | - |
| MTCA | SAPSE | 170.09 | −43.73 | 3 | Poor | - | - | - | - | - | - | - | - | - | - | - |
| MTJA | SAPSE | 170.47 | −43.99 | 27 | Good | 2.68 | 24.3 | ±2.9 | 1.670 | ±0.124 | - | - | - | 6.60 | 56.4 | ±1.9 |
| NNZ | NZNSN | 173.38 | −41.22 | 29 | Good | 3.98 | 29.5 | ±5.2 | 1.828 | ±0.185 | 2.32 | 21.5 | ±2.5 | 8.64 | 75.9 | ±2.8 |
| ODZ | NZNSN | 170.65 | −45.05 | 37 | Good | 3.05 | 24.0 | ±2.1 | 1.788 | ±0.105 | - | - | - | 6.02 | 54.6 | ±4.0 |
| QRZ | NZNSN | 172.53 | −40.83 | 31 | Good | 3.40 | 30.0 | ±0.7 | 1.713 | ±0.028 | - | - | - | 5.55 | 55.3 | ±2.2 |
| QRZA | SAPSE | 172.53 | −40.83 | 25 | Good | 3.52 | 29.8 | ±2.1 | 1.725 | ±0.061 | 2.31 | 20.0 | ±1.8 | 5.69 | 50.8 | ±1.9 |
| SHEA | SAPSE | 171.88 | −43.39 | 8 | Medium | 3.80 | 29.3 | ±0.6 | 1.813 | ±0.028 | - | - | - | - | - | - |
| THZ | NZNSN | 172.91 | −41.76 | 30 | Good | 3.67 | 29.5 | ±0.7 | 1.767 | ±0.032 | 2.45 | 22.0 | ±1.7 | 8.21 | 77.2 | ±2.6 |
| TOBA | SAPSE | 175.54 | −39.23 | 2 | Poor | - | - | - | - | - | - | - | - | - | - | - |
| TOPA | SAPSE | 172.91 | −41.76 | 6 | Medium | - | - | - | - | - | - | - | - | - | - | - |
| TUZ | NZNSN | 169.63 | −45.96 | 36 | Good | 2.53 | 23.1 | ±1.0 | 1.690 | ±0.035 | - | - | - | 3.97 | 32.9 | ±2.9 |
| WHZ | NZNSN | 167.95 | −45.89 | 31 | Medium | 4.60 | 36.8 | ±1.8 | 1.767 | ±0.069 | - | - | - | - | - | - |
| WKZ | NZNSN | 169.02 | −44.83 | 9 | Poor | - | - | - | - | - | - | - | - | - | - | - |
| WVZ | NZNSN | 170.74 | −43.08 | 32 | Good | 3.22 | 29.8 | ±1.1 | 1.660 | ±0.040 | - | - | - | 6.41 | 59.1 | ±2.7 |

[a]Dashes indicate that corresponding feature could not be mapped using available receiver functions.

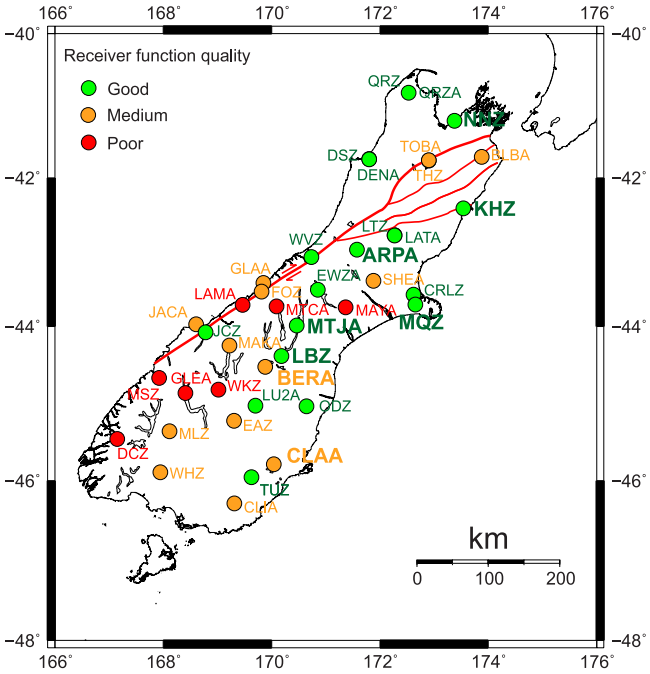


**Figure 3.** Distribution of seismic stations and quality of receiver functions in South Island, New Zealand. Four-letter station codes denote stations in the SAPSE network, and three-letter station codes denote stations in the NZNSN, with the exception of station CRLZ, which belongs to NZNSN. Green, orange, and red dots indicate stations with good, medium, and poor quality of receiver function, respectively. Receiver function for stations KHZ, LBZ, MTJA, ARPA, MQZ, NNZ, BERA, and CLAA are shown on Figure 4.

quality of receiver functions, and are shown with red dots on Figure 3. Stations with good quality have very good agreement of conversion depths on the receiver functions, high coherence, a good quality stack, and in general have larger number of receiver functions. Medium quality of seismic stations is qualitatively defined as an intermediate category between the two end-members.

[18] There is a strong geographical variation of the receiver function quality through the South Island (Figure 3). Receiver functions have the best quality in the north and east portion of the island, and in general to the east from the longitude 170°. Most of the stations in the southern portion of the island (Figure 3), especially in the Otago and Fiordland regions, produce poor quality receiver functions, possibly due to complex crustal structure in this region. Multiple crustal scatterers, such as heterogeneous geology and complex dipping structures can create numerous conversions, producing very noisy receiver functions that are difficult to analyze and interpret. In addition, this region is seismically very active, with frequent small magnitude earthquakes which can create noisy records and causing poor quality of receiver functions.

### 3.2. Receiver Function Analysis

[19] Although seismic data for permanent NZNSN network and several temporarily deployed seismic networks is readily available for the South Island, receiver functions have not been widely utilized for definition of lithospheric structure in this region, especially in a three-dimensional sense. In an early study, *Calhaem et al.* [1977] use conversion from S to P phase at the base of crust from a local earthquake to define crustal thickness in Mount Huxley area. *Parker* [1999] studied just seven stations throughout the South Island to determine Moho depths. *Savage et al.* [2007] use receiver functions to study structure of Hikurangi subduction zone in the North Island, which yields some information for only the northernmost part of the South Island. To our knowledge, only available three-dimensional models of crustal thickness are based on tomographic studies that utilize first arrivals only and define Moho discontinuity as an isovelocity surface [*Kohler and Eberhart-Phillips*, 2002; *Eberhart-Phillips and Bannister*, 2002].

[20] Receiver functions provide important direct observations of velocity discontinuities and as such provide valuable additional constraints for studies of lithospheric structure. The South Island is recognized as a region with very complex tectonics [*Walcott*, 1998] and heterogeneous lithospheric structure [*Scherwath et al.*, 2003]. The density of available three-component seismic network and the nature of the receiver function method do not enable us to account for all the complexity and our analysis is based on several premises:

[21] 1. We explore relatively long-wavelength, low-resolution lithospheric structure, with the spatial resolution on order of 50 to 100 km. Receiver functions give local estimates of lithospheric structure, and interpolated values between stations have uncertainty which increases with the distance from seismic stations.

[22] 2. Although crust in the region of the South Island has heterogeneous structure with multiple crustal velocity layers [*Scherwath et al.*, 2003; *Van Avendonk et al.*, 2004], we implement methodology which defines depths to crustal interfaces using average crustal velocities. Although average crustal velocity might vary in different areas of the South Island [*Van Avendonk et al.*, 2004; *Melhuish et al.*, 2005, *Scherwath et al.*, 2003], we use same value of 6.3 km/s for all stations, avoiding introduction of additional level of uncertainty that cannot be constrained using receiver functions. Slightly different average crustal velocity would introduce minor changes to our depth estimates, as shown by equation (7).

[23] 3. The assignment of a particular lithospheric feature, such as Moho or crustal interface, to a conversion detected using H-Vp/Vs methodology is interpretative and based on a set of qualitative criteria defined by authors, which introduces a certain level of uncertainty in analysis. We interpret the strongest and most coherent conversion as Moho. It was recognized that lower crust in the South Island has a strong seismic response [*Bourguignon et al.*, 2007; *Woodward*, 1979] that could possibly overwhelm the Moho signature in certain locations. In locations where local geological structures, such as dipping structures, produce strong coherent signal on receiver functions, uncertainty in interpretation of regional structure, such as Moho interface, increases.

[24] We utilize primary P-to-S conversion and associated multiples to identify following features on receiver func-

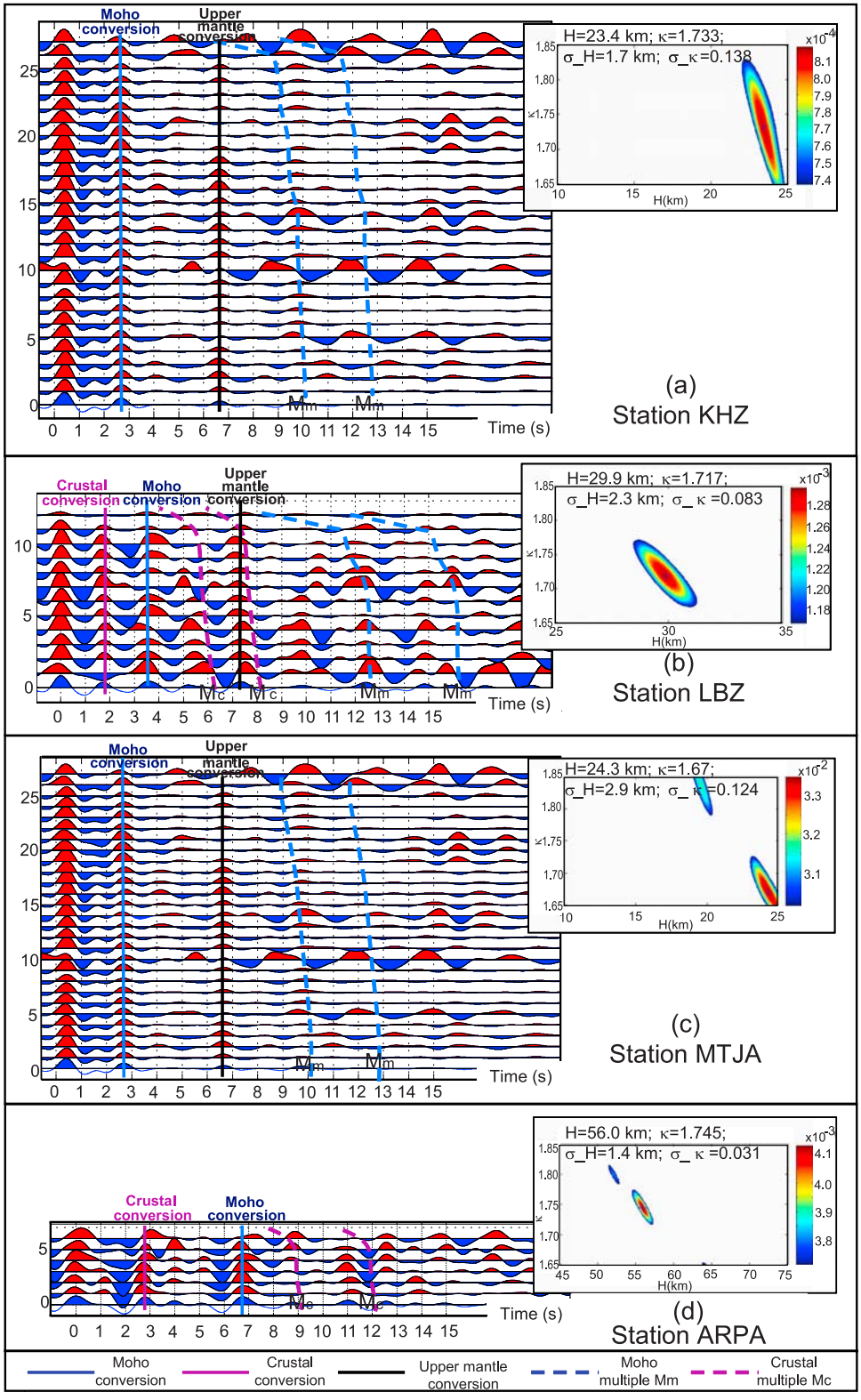


**Figure 4.** Sample receiver functions for stations (a) KHZ, (b) LBZ, and (c) MTJA, (d) ARPA, (e) MQZ, (f) NNZ, (g) BERA, and (h) CLAA. Each plot represents selected receiver functions for one station and multiple seismic events, ordered by increasing ray parameter p from bottom to top. Horizontal scale is receiver function reduced S-P time (s) and vertical scale is number of receiver functions. A principle component filter has been applied to the receiver function. Thick lines show Moho (blue), upper mantle (black), and crustal (purple) conversion, and dashed lines show predicted position of corresponding multiples. Insert plots show determined Moho depth H (km) and $\kappa$ (Vp/Vs ratio), and associated errors $\sigma$_H and $\sigma$_$\kappa$. Colors indicate coherency of stack.

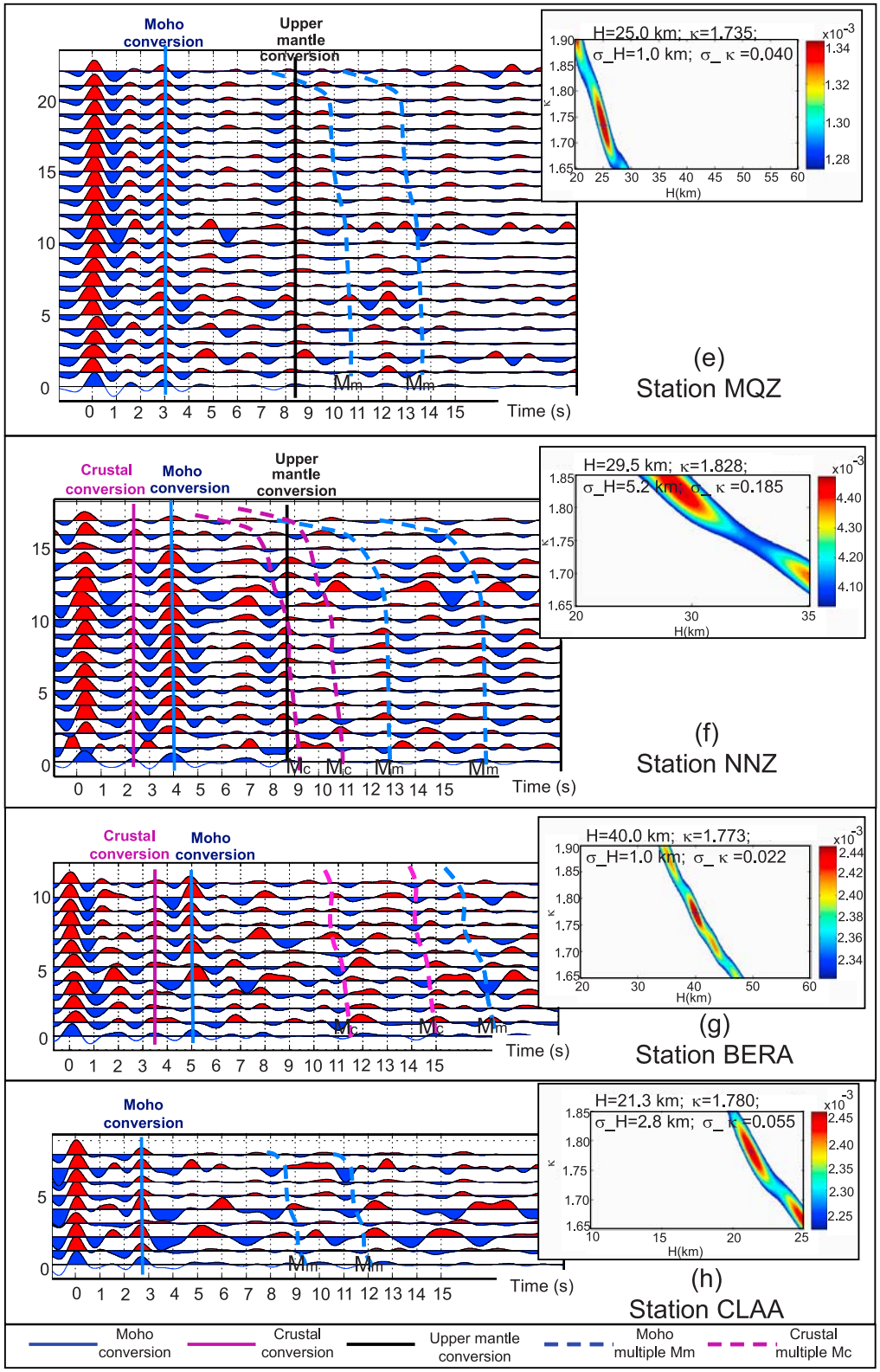


**Figure 4.** (continued)

tions for stations with good or medium quality: (1) Moho discontinuity conversion, (2) crustal conversion features, and (3) upper mantle conversion features (Table 1). As examples, receiver functions for eight stations are shown in Figure 4. Six stations are characterized to have good quality (stations KHZ, LBZ, MTJA, ARPA, MQZ, NNZ), and two medium quality of receiver functions (BERA, CLAA).

[25] The strength of the multiple phases varies from station to station. Although we implemented the H-Vp/Vs

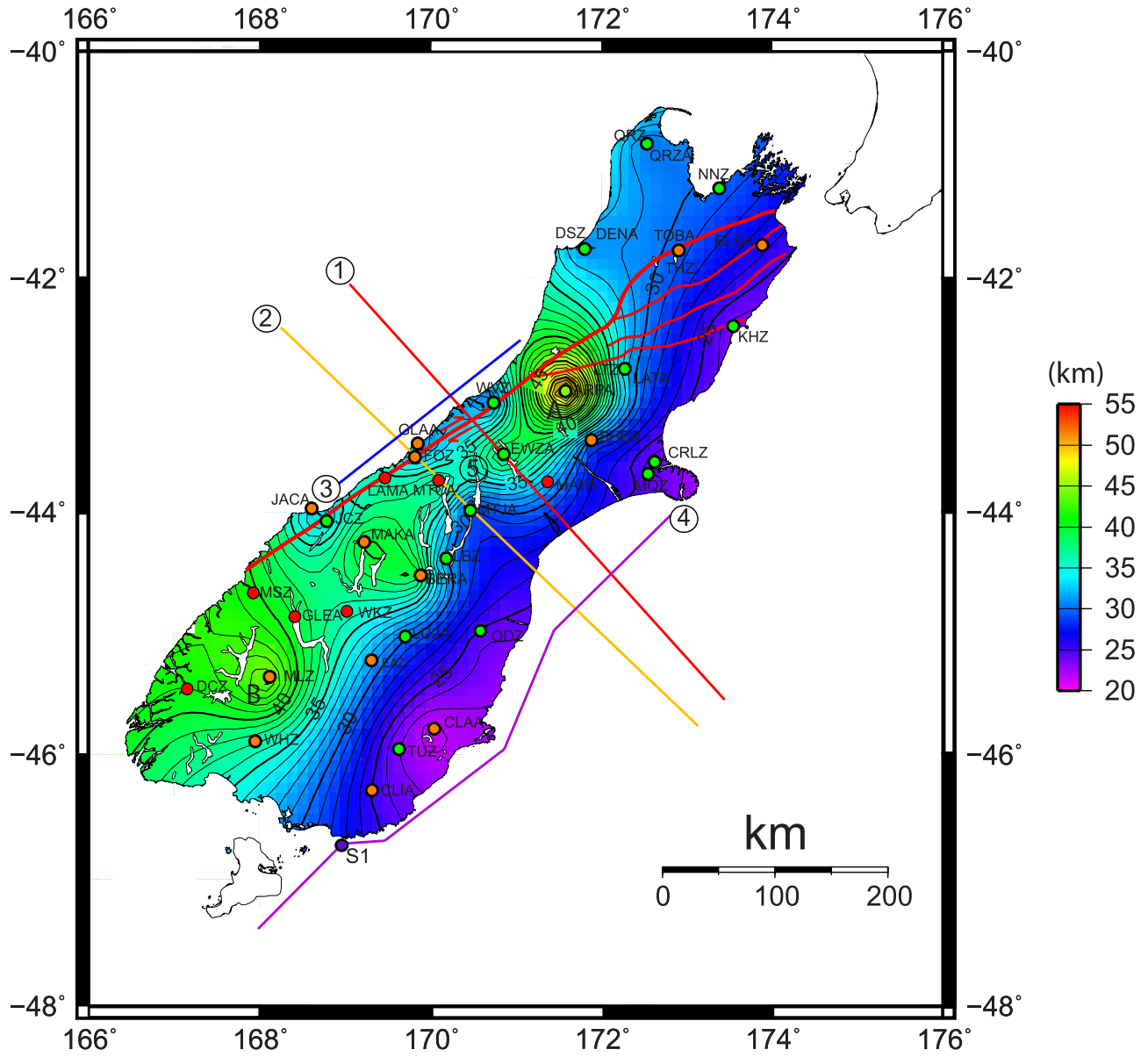


**Figure 5.** Map of crustal thickness calculated using the H-Vp/Vs method and average crustal velocity of 6.3 km/s. Regions with the thickest crust are shown with letters A and B. Green, orange, and red dots indicate stations with good, medium, and poor quality of receiver function, respectively. Contour interval is 1 km. Line 1 is SIGHT transect 1 [*Van Avendonk et al.*, 2004], line 2 is SIGHT transect 2 [*Scherwath et al.*, 2003], line 3 is SIGHT Profile 3w [*Melhuish et al.*, 2005], line 4 is SESI profile [*Godfrey et al.*, 2001; *Mortimer et al.*, 2002] with point S1 located offshore Murihuku terrain, and 5 is Lake Pukaki area [*Woodward*, 1979].

method, crustal thickness and Vp/Vs ratio for some of the stations were determined mostly using primary P-to-S conversion since multiples are very weak. For example, for seismic stations LBZ (Figure 4b) and NNZ (Figure 4f) both Moho and crustal multiples are relatively strong. However, for stations MTJA (Figure 4c) and CLAA (Figure 4h) multiple phases are much weaker, causing H-Vp/Vs estimate to be based mostly on primary conversion.

[26] The Moho discontinuity typically has the strongest signature on most of the receiver functions (Figure 4). Receiver functions also indicate the existence of a crustal conversion for some of the stations. For example, it is clear for the stations LBZ, MQZ, NNZ and BERA (Figure 4), but it is not evident on all stations. Once we determine the conversions and predict corresponding multiples for the Moho discontinuity and the crustal conversion, it is possible to systematically map conversion features in the upper mantle. For example, stations LBZ, MTJA, MQZ and NNZ (Figure 4) show sub-Moho conversion that is not coincident with any of the predicted multiples, which indicates presence of upper mantle conversion feature. A

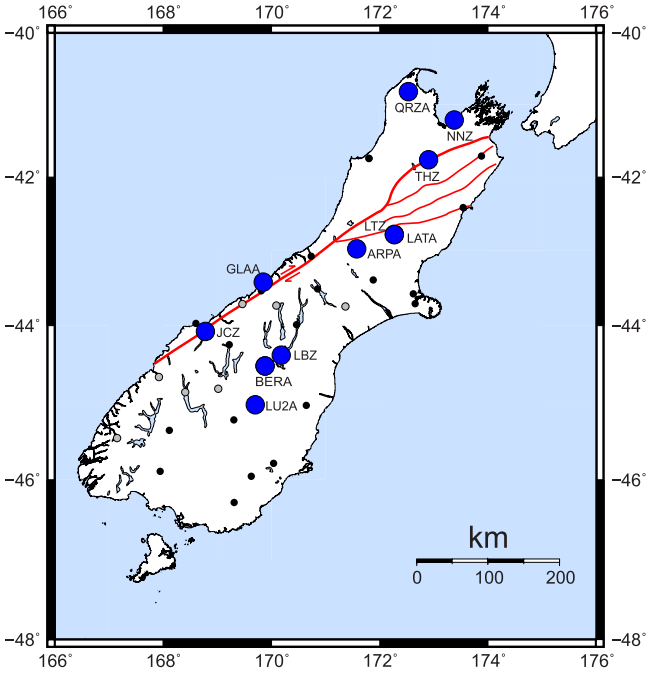


**Figure 6.** Position of stations with developed crustal conversions. Stations that have well-developed conversion in the crustal section are shown with large blue circles. Stations with acceptable seismic quality that are used in the analysis are shown with black circles. Stations with poor quality not used in the analysis are shown with gray dots.

total of 16 stations show evidence for the existence of such a strong upper mantle conversion feature (Table 1).

### 3.3. Crustal Structure

[27] On the basis of our analysis of receiver functions, using the H-Vp/Vs method and an average crustal velocity of 6.3 km/s, crustal thickness estimates in the South Island varies from 21 km to 56 km (Figure 5 and Table 1). The region with the thinnest crust is located on the Pacific plate, on the east coast of the South Island with the average thickness of approximately 25 km (Figure 5). The crustal thickness progressively increases toward the central portion of the Island, and the Moho is the deepest along the axis of the Southern Alps, adjacent to the Alpine Fault (Figure 5). The region with a maximum crustal thickness of 56 km (marked with A on Figure 5) in the northern central South Island is roughly coincident with location of where the Alpine fault splays into a number of major faults toward the north South Island. Average crustal thickness in northern South Island and central west coast is around 30 and 35 km, respectively. Maximum crustal thickness in Otago and Fiordland area is approximately 45 km, but this value is less well constrained considering relatively poor quality of the receiver functions (Figure 3).

[28] Receiver functions define the crustal root in the central portions of the South Island, with the root axis running approximately parallel to the Alpine fault at the distance of 20–50 km east from the surface trace of the fault (Figure 5). The width of the root increases from north to the south in the direction perpendicular to the Alpine fault. It is widest in the Otago and Fiordland regions (area marked B in Figure 5), which might indicate more distributed deformation in this region. The crustal root appears asymmetric, with a steeper western and a gentler eastern side.

[29] Previous 2-D studies define higher resolution lithospheric structure along several transects in the South Island and provide a good comparison for the crustal structure determined using receiver functions (Figure 5). There is good agreement between the receiver function results and several 2-D studies:

[30] 1. In the central South Island (Figure 5), the estimated crustal thickness on the SIGHT transect 1 [*Van Avendonk et al.*, 2004] is 37 km. The station EWZA located few kilometers northeast from the transect 1 (Figure 5) gives crustal thickness estimate of 40.6 ± 2.1 km. Small differences in depth between these two observations can be explained by differences in velocity models, as described in equation (7).

[31] 2. *Godfrey et al.* [2001] and *Mortimer et al.* [2002] analyze seismic, gravity and magnetic data collected on 550 km long South East South Island (SESI) profile. *Godfrey et al.* [2001] define seismic velocity model and measure a Moho depth of 25 km in the Dunedin region. *Mortimer et al.* [2002] model Moho depths of 22–32 km along the SESI profile using seismic reflection, magnetic and gravity data, with the maximum depth being observed in the offshore Murihuku terrain (point S1 on Figure 5), and shallowing of the Moho toward both northeast and southwest parts of the profile. Stations CLIA, TUZ, CLAA and ODZ in Dunedin region are located along an onshore profile which is roughly parallel to the SESI line (Figure 5), with crustal thickness values determined from receiver functions varying between 21.3 and 25.1 km (Table 1), which are within the range of crustal thickness values given by *Mortimer et al.* [2002] and *Godfrey et al.* [2001].

[32] 3. *Melhuish et al.* [2005] defined a Moho depth of 26–30 km along offshore SIGHT profile 3w (Figure 5). Receiver function from stations WVZ and GLAA indicate depths of 29.8 and 29.5 km (Table 1), respectively, which

**Table 2.** Relationship Between Moho Depths Determined Using Radial and Transverse Receiver Functions

| | Moho Depth, km | | |
|---|---|---|---|
| Station | Transverse | Radial | Ratio of Moho Depth (T/R) |
| ARPA | 48.5 | 56 | 0.87 |
| CRLZ | 32.6 | 23.2 | 1.41 |
| DENA | 34.5 | 30.3 | 1.14 |
| DSZ | 33.7 | 30.2 | 1.12 |
| EWZA | 40 | 40.6 | 0.99 |
| JCZ | 30 | 32 | 0.94 |
| KHZ | 21.2 | 23.2 | 0.91 |
| LATA | 34.5 | 31.9 | 1.08 |
| LBZ | 27 | 29.9 | 0.90 |
| MQZ | 25 | 25 | 1.00 |
| MTJA | 24.5 | 24.3 | 1.01 |
| NNZ | 29.2 | 29.5 | 0.99 |
| ODZ | 28.9 | 24 | 1.20 |
| QRZ | 33.5 | 30 | 1.12 |
| QRZA | 30.1 | 29.8 | 1.01 |
| THZ | 36 | 29.5 | 1.22 |
| TUZ | 40.5 | 23.1 | 1.75 |

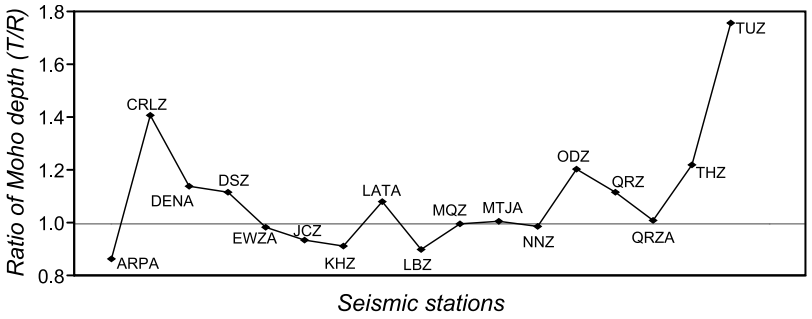


**Figure 7.** Relationship between Moho depths determined using transverse and radial receiver functions. When transverse receiver function indicates bigger Moho depth than radial receiver function, ratio is higher than 1.

fits within the bound of values defined by *Melhuish et al.* [2005].

[33] 4. *Woodward* [1979] modeled gravity data along several profiles perpendicular to the axis of Southern Alps, determining maximum crustal thickness of 40 km in Lake Pukaki region (Figure 5), postulating that previously determined thickness of 32 km using S-P conversion from a local event [*Calhaem et al.*, 1977] is probably attributable to a strong lower crust interface. Our interpolated value of 38 km in this region (Figure 5) is similar to the one provided by *Woodward* [1979].

[34] In addition, crustal thickness map derived from our receiver functions study correlates relatively well with results of previous three-dimensional studies of crustal structure [*Kohler and Eberhart-Phillips*, 2002; *Eberhart-Phillips and Bannister*, 2002] in the southern and central portions of the South Island. *Kohler and Eberhart-Phillips* [2002] also find that the crustal root widens in Otago, and estimate similar average thickness of approximately 45–50 km in the area marked with B in Figure 5. In the region with poor receiver function quality in the Fiordland region, they find a thickness of approximately 56 km in the southwest corner of the island, which is smaller than our extrapolated value and can be explained by lack of receiver function coverage, and poor quality of seismic records in this region.

[35] There are, however, a few discrepancies between our results and previous studies:

[36] 1. Along transect 2, maximum crustal thickness is 44 km [*Scherwath et al.*, 2003], which is larger than maximum thickness of 37 km determined using receiver functions (Figure 5). This discrepancy can be explained by poor spatial coverage in this part of the transect 2, where station MTCA located directly on the profile has poor quality of the receiver functions, and stations EWZA and MAKA are located 60 and 80 km away, respectively, in the direction perpendicular to the transect 2. However, station MTJA is located directly on the transect 2, and gives estimate of crustal thickness that is approximately 10 km smaller than one estimated by *Scherwath et al.* [2003]. Receiver functions for this station have very good quality (Figure 4c), with depth uncertainty that is significantly smaller than difference of these two results (Table 1). This discrepancy could be potentially caused by local crustal structure, where impedance contrast in the lower crust can be higher than one at the crust-mantle boundary. If the depth difference is to be explained by changes in Vp or $\kappa$, they would need to change by 2.3 km/s and 0.25 respectively, both of which seem unreasonable.

[37] 2. Crustal thickness of 56 km at station ARPA is higher than one established in the same region by *Kohler and Eberhart-Phillips* [2002]. Since the seismic conversion interpreted as Moho conversion is very coherent, with good quality of receiver functions (Figure 4d), we are confident that depth estimate of the conversion feature is reasonable. It is possible that a local crustal or mantle structure, such as steeply dipping faults, is generating this converted phase, which represents the strongest phase at the station. Again only extreme changes in average crust Vp or $\kappa$ will significantly reduce the depth.

[38] The discussion given above demonstrates that estimates of crustal thickness from receiver functions correlate well with many previously published studies. Receiver functions use direct detection of conversions from the Moho interface, complementing 3-D tomographic analysis, and providing 3-D coverage in areas where high-resolution profile data have not been collected. Discrepancies detected at few locations may be caused by: intrinsic limitations of receiver function methodology, where 3-D interpolation quality in the regions of poor spatial coverage and poor quality of seismic records decreases with increasing distance from seismic stations; or by local lithospheric structure where strong impedance contrast in the lower crust or local structures cause strong conversions detected on the receiver functions.

[39] Clear evidence of seismic conversion within the crustal section has been mapped on twelve stations in the region of the South Island (Table 1). With the exception of two stations in the northern South Island, they are located in the alpine portion of the island, adjacent to the Alpine fault (Figure 6), in the region with increased crustal thickness. The depth of the crustal conversions is between 13 and 26 km. Previous studies identify several features that can be related to these conversions. *Henrys et al.* [2004] identify a very reflective lower crust that bends beneath the South Alps. *Scherwath et al.* [2003] find thickening of the lower crust on the SIGHT transect 2 in the central portion of the orogen, which might explain the preferential localization of crustal conversions found on the receiver functions closer to the Alpine Fault and in the axial region of the South Island. *Davey et al.* [1998] find midcrustal to lower crustal reflective zone that is highly conductive, probably corresponding to a fluidized weak zone, with the crustal reflectivity that fades away with increased crustal

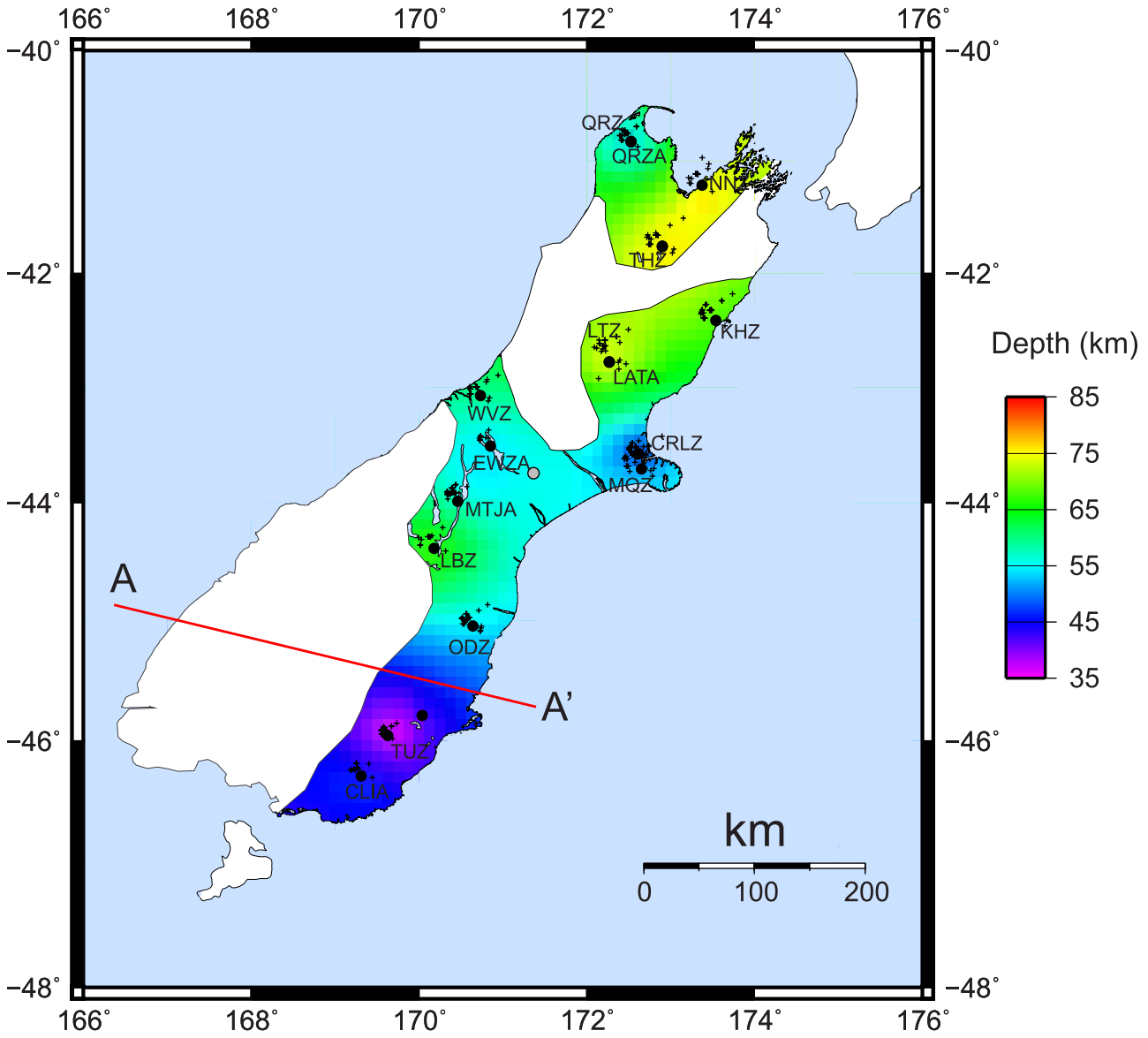


**Figure 8.** Depth structure of the uppermost mantle conversion calculated using average crustal velocities of 6.3 km/s and upper mantle velocities of 8.1 km/s. Crosses show position of piercing points for upper mantle conversions and indicate stations that have uppermost mantle conversion present. Stations with acceptable seismic quality are shown with black circles. Stations with bad seismic quality are shown with gray dots. A schematic cross section through profile A-A' is shown on Figure 10.

thinning. Since seismic conversions in the crustal sections do not appear on stations located on the east coast of the South Island in the region with thin crust, it is likely that these features are related to the reflective and conductive zone interpreted by *Davey et al.* [1998].

[40] We also analyzed transverse receiver function for a set of 18 seismic stations that has the best quality of receiver functions in both radial and transverse direction. There is a significant difference in the values of the Moho depth determined using transverse and radial receiver functions (Table 2). The ratio between Moho depths determined using transverse versus radial receiver functions varies from 0.87 to 1.75 (Table 2). A majority of the station have Moho depth determined from transverse receiver functions larger than the one determined for the radial receiver functions (Figure 7), which can be due to higher velocities in the transverse direction. Since crustal root and associated structures in the upper mantle run in the direction parallel to the Alpine fault, and roughly in the same direction as transverse components, it is possible that this difference is caused by lithospheric anisotropy. *Melhuish et al.* [2005] determined that upper mantle anisotropy is around 10%, which is sufficient to account for the differences at the most of the stations.

### 3.4. Uppermost Mantle Conversions and Evidence for Possible Tectonic Underplating

[41] Receiver functions for 16 stations in the South Island (Table 1) show strong evidence for the existence of a prominent P-to-S conversion in the upper mantle. The extent of the upper mantle conversion, as mapped by receiver functions, is shown on Figure 8. There are

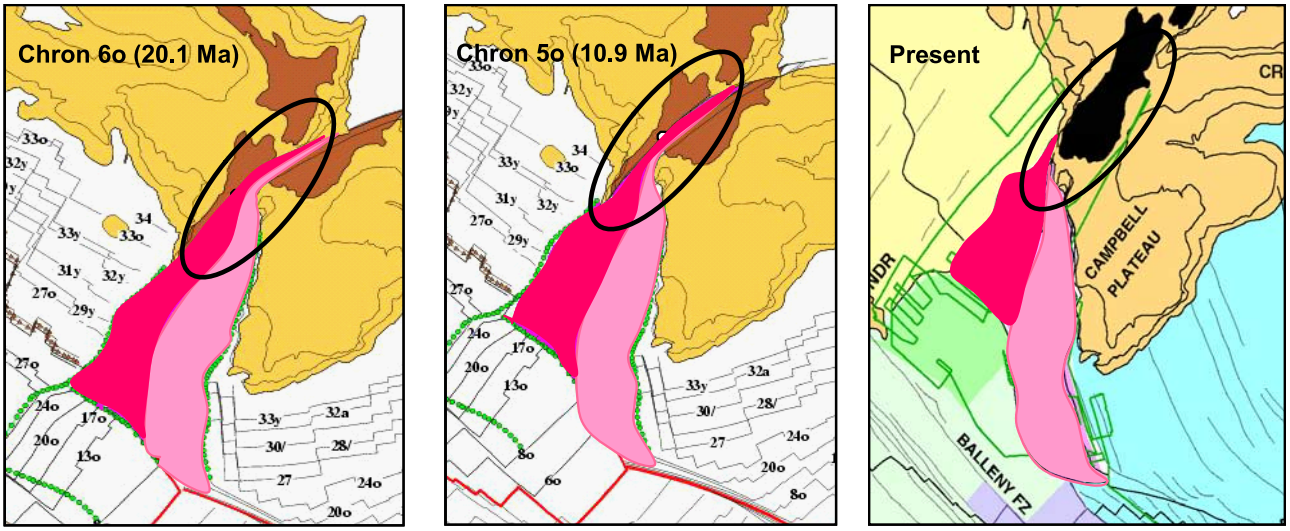


**Figure 9.** Ocean provinces reconstruction in last 20 Ma (adapted from *Cande and Stock* [2004b]). A part of late Oligocene–Miocene oceanic crust created by spreading between the Pacific (light pink) and Australian (darker pink) plates is missing in the present-day crust budget (indicated with the ellipse). We propose that this portion of the crust is tectonically underplated under the South Island.

two separate regions with well-developed upper mantle conversion: (1) a small patch in the north South Island and (2) a large, possibly continuous, feature on the east coast and in the central region of the South Island. The depth of the conversion, calculated using a simple velocity model with average crustal and upper mantle velocities of 6.3 and 8.1 km/s, respectively, vary between 33 and 83 km (Table 1), placing this feature in the uppermost mantle, just below the Moho discontinuity. This feature is most evident on the east coast and in the central region of the South Island.

[42] Uppermost mantle conversions have been previously explored in a number of receiver functions studies worldwide. Most of the studies deal with imaging of active subducting zones, and provide additional constraints on the subduction geometry and contribute to the understanding of interaction between slab and mantle wedge [e.g., *Ai et al.*, 2005; *Owens et al.*, 1988]. Few studies explore regions other than active subduction zones where upper mantle conversions can be related to relict tectonic features. *Asencio et al.* [2003] find a phase conversion from a subhorizontal velocity discontinuity in Scotland, which correlates well with a regionally extensive seismic reflector from deep marine seismic reflection and wide-refraction profiles. This feature could be attributed to eclogitized oceanic crust that belongs to a relic subduction zone proposed by *Warner et al.* [1996]. *Bostock* [1999] also describes velocity discontinuities in the uppermost mantle, arguing that they can be tied to tectonic history of a specific location.

[43] Relative spatial separation of the two regions with the upper mantle conversion, and slightly different depth patterns (Figure 8) suggest that they might be associated with different subsurface features. It is likely that the northern patch is associated with the Hikurangi subduction zone, and that mantle conversions represent conversions from the top of the subducting Pacific plate. However, the sense of the dip of upper mantle conversion is opposite than it would be expected from northwesterly subduction. It is possible that the depth in this regions is not well constrained by three stations, or that the simple 1-D velocity model we employed to calculate depths is not appropriate in this environment.

[44] We propose two possible models for the large apparently continuous upper mantle conversion on the east coast and in the central portions of the South Island: (1) uppermost mantle conversions could be associated with the tectonically underplated late Oligocene-Miocene oceanic crust, (2) upper mantle conversions are caused by structures associated with subduction of terranes accreted to Gondwanaland.

### 3.4.1. Model 1: Evidence for Tectonic Underplating of Late Oligocene–Miocene Oceanic Crust

[45] *Cande and Stock* [2004a, 2004b] revised the plate motion model for this region and determined that a significant amount of the seafloor, mostly corresponding to a part of the Australian plate (Figure 9, shown in darker pink) created by the late Oligocene–Miocene Australia-Pacific spreading, is missing in the present-day crust budget. On the basis of the reconstructions (Figure 9), this crust is mostly preserved in the interval between 20 and 10 Ma ago, and is missing in the budget in the last 10 Ma. In this time interval, a jump of the instantaneous pole of rotation between the Pacific and Australian plates toward west-southwest occurred [*Cande and Stock*, 2004a, 2004b]. *Sutherland et al.* [2000] also recognize that at least of $3{\cdot}10^4$ km$^2$ of the late Oligocene-Miocene oceanic crust is still unaccounted for. In one of their models, *Sutherland et al.* [2000] propose that the oceanic lithosphere has been detached from the Australian plate by tearing at the Puysegur subduction zone, and postulate that is should be located at depths of 150 km.

[46] The extent of the large continuous upper mantle conversions (Figure 8) is well correlated with the outline of the missing oceanic crust (Figure 9), and its position is analogous to the modeled position of the unaccounted for oceanic lithosphere proposed by *Sutherland et al.* [2000]. We propose a model in which the continuous upper mantle reflector on the southeast side of the Island is attributed to

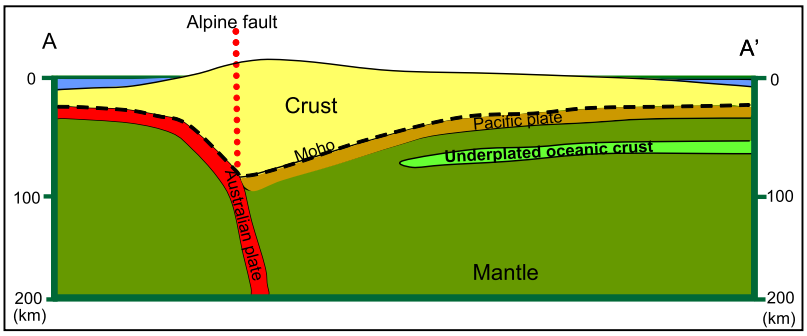


**Figure 10.** Schematic cross section through the south portion of the South Island. The position of the cross section is shown on Figure 8. The tectonically underplated oceanic crust is detached from the Australian plate and positioned in the upper mantle.

late Oligocene–Miocene oceanic crust created by the spreading between the Pacific and Australian plates, which has been detached from the Australian plate and overridden by New Zealand (Figure 10). We will use term tectonic underplating in this paper to describe this oceanic crust that is now located in the uppermost mantle under the South Island. Tectonic underplating terminology was introduced by *Platt* [1993] to describe a tectonic process which adds new material under a region. This model is an extension of a model proposed by *Sutherland et al.* [2000], in which the late Oligocene–Miocene oceanic crust detached from the Australian plate and is now completely decoupled from the Australian plate. The slab became stagnant in the upper mantle upon the detachment from the Australian plate, and it has been overridden by the South Island. Receiver function analysis indicates that the depth of the oceanic crust is between 33 and 83 km, significantly shallower than the depth proposed by *Sutherland et al.* [2000].

#### 3.4.2. Model 2: Evidence for Features Created by Cretaceous Subduction of Gondwanaland

[47] There is a general increase of the depth of upper mantle conversion from southwest toward northeast of a continuous upper mantle conversion in the southern and central portions of the island (Figure 8). This direction is consistent with the direction of paleosubudction zone related to the subduction Gondwanaland terranes in the region of the South Island [*Davey*, 2005]. *Davey* [2005] examined lower crustal and upper mantle reflectivity in the region of Stewart Island, south of the South Island, using multichannel seismic data. Lower crustal and upper mantle seismic reflections were attributed to terranes sutures associated with paleosubduction of Gondwanaland margin [*Davey*, 2005], with approximate northwest-southeast orientation. This orientation is subparallel to terrane boundaries in the southeast South Island, and the estimated dip direction is similar to the dip of inferred paleosubduction at the Gondwanaland margin [*Davey*, 2005]. *Melhuish et al.* [2005] analyzed a SIGHT profile parallel to the Alpine fault on the Australian plate and determined the presence of a strong northeast dipping reflection beneath Moho, with depths between 55 and 110 km, proposing a model in which these reflections are caused by structures related to Paleozoic subduction at the Gondwanaland margin. The orientations of inferred northeast dipping paleosubduction zone in the Western Province [*Davey*, 2005] and mantle structures in the offshore region in the western South Island [*Melhuish et al.*, 2005] is similar, and they might be related to the same suture [*Davey*, 2005]. The structural orientation of the uppermost mantle conversion determined in this study is very similar to the orientation of offshore reflective features determined in the studies of *Davey* [2005] and *Melhuish et al.* [2005], and it is therefore possible that upper mantle conversion features related to structures created by long-lived subduction that ceased 130–80 Ma [*Sutherland*, 1999]. This model requires that seismic fabric of the lithosphere is preserved for a relatively long time since Cretaceous.

## 4. Conclusions

[48] Analysis of more than 700 receiver functions for 42 stations in the South Island, New Zealand, provide additional constraints on the three-dimensional structure of the crust and upper mantle, and complement previous 2-D and 3-D studies of lithospheric structure. The region of the thickest crust is located along the axis of the Southern Alps, approximately 20 to 50 km east from the Alpine fault. Receiver functions show evidence for the existence of the axial crustal root with asymmetric structure, with width that increases from north to south in the direction perpendicular to the Alpine fault. The crustal root is the widest in the Otago area which might indicate broader area of deformation in this region. Crustal thickening in the South Island developed in a response to the convergent component of motion on the Alpine fault and subduction in the Fiordland region. Axial portions of the South Island show evidence for strong conversions in the midcrustal section, which correlates well with the previously imaged reflective and highly conductive midcrustal to lower crust layer, which disappears with decreasing overall crustal thickness toward the east. There is general agreement of crustal structure defined using receiver functions and other studies, with two discrepancies noted in the discussion section.

[49] Strong conversions located in the uppermost mantle can be spatially separated into a small region in the north, and a large apparently continuous feature located on the east side and in the central portions of the South Island. A relatively small region with upper mantle conversions in the north can be attributed to the Hikurangi subduction, with conversions probably occurring at the top of the subducting

Pacific plate. We propose two different models for structure causing a large continuous upper mantle conversion. In the first model, conversions are attributed to underplated late Oligocene–Miocene oceanic crust that has been created by spreading between the Pacific and Australian plate. The crust has been detached from the Australian plate, and has been since overridden and underplated under the South Island. In the second model, upper mantle conversions can be attributed to the paleosubduction on the Gondwanaland margin in the region of the South Island. We favor the first model because of several reasons. First, the outline of the upper mantle conversion and estimate of its surface area relates closely to the reconstructions of the late Oligocene–Miocene oceanic crust that is unaccounted for in the present-day crust budget [*Cande and Stock*, 2004b] and estimates of its missing surface area [*Sutherland et al.*, 2000]. Additionally, second model requires that lithospheric seismic fabric of Gondwanaland margin subduction is preserved for a relatively long time since Cretaceous, and it is likely that the signature of the late Oligocene–Miocene oceanic crust is preserved in the area of the South Island.

[50] **Acknowledgments.** We want to acknowledge New Zealand GeoNet project and its sponsors EQC, GNS Science, and FRST for providing data from NZNSN; Monica Kohler for providing the SAPSE data; David Okaya for providing three-component SIGHT data; Joann Stock for providing plate reconstruction data and useful discussion about the tectonics of New Zealand; and Zhimei Yan for help with processing of receiver function data. This paper has benefited from discussions with Fred Davey, Brian Davies, and Bruce Luyendyk and comments from two anonymous reviewers.

## References

Ai, Y., D. Zhao, X. Gao, and X. Weiwei (2005), The crust and upper mantle discontinuity structure beneath Alaska inferred from receiver functions, *Earth Planet. Sci. Lett.*, *150*, 339–350.

Asencio, E., J. H. Knapp, T. J. Owens, and G. Helffrich (2003), Mapping fine-scale heterogeneities within the continental mantle lithosphere beneath Scotland: Combining active- and passive-source seismology, *Geology*, *31*(6), 477–480, doi:10.1130/0091-7613(2003)031<0477:MFHWTC>2.0.CO;2.

Bostock, M. G. (1999), Seismic imaging of lithospheric discontinuities and continental evolution, *Lithos*, *48*, 1–16, doi:10.1016/S0024-4937(99)00020-1.

Bourguignon, S., T. A. Stern, and M. K. Savage (2007), Crust and mantle thickening beneath the southern portion of the Southern Alps, New Zealand, *Geophys. J. Int.*, *168*, 681–690, doi:10.1111/j.1365-246X.2006.03208.x.

Calhaem, I. M., A. J. Haines, and M. A. Lowry (1977), An intermediate-depth earthquake in the central region of the South Island used to determine a local crustal thickness, *N. Z. J. Geol. Geophys.*, *20*(2), 353–361.

Cande, S. C., and J. M. Stock (2004a), Pacific-Antarctic motion and the formation of the Macquarie plate, *Geophys. J. Int.*, *157*, 399–414, doi:10.1111/j.1365-246X.2004.02224.x.

Cande, S. C., and J. M. Stock (2004b), Cenozoic reconstructions of the Australia-New Zealand-South Pacific sector of Antarctica, in *The Cenozoic Southern Ocean: Tectonics, Sedimentation and Climate Change Between Australia and Antarctica*, *Geophys. Monogr. Ser*, vol. 151, edited by N. F. Exon, J. P. Kennett, and M. J. Malone, pp. 5–18, AGU, Washington, D. C.

Davey, F. (2005), A Mesozoic crustal structure on the Gondwana margin in the New Zealand region, *Tectonics*, *24*, TC4006, doi:10.1029/2004TC001719.

Davey, F. J., et al. (1998), Preliminary results from a geophysical study across a modern continent-continent collisional plate boundary—The Southern Alps, New Zealand, *Tectonophysics*, *288*, 221–235, doi:10.1016/S0040-1951(97)00297-7.

Eberhart-Phillips, D., and S. Bannister (2002), Three-dimensional crustal structure in the Southern Alps region of New Zealand from inversion of local earthquake and active source data, *J. Geophys. Res.*, *107*(B10), 2262, doi:10.1029/2001JB000567.

Eberhart-Phillips, D., and M. Reyners (1997), Continental subduction and three-dimensional crustal structure: The northern South Island, New Zealand, *J. Geophys. Res.*, *102*(B6), 11,843–11,861, doi:10.1029/96JB03555.

Eberhart-Phillips, D., and M. Reyners (2001), A complex, young subduction zone imaged by three-dimensional seismic velocity, Fiordland, New Zealand, *Geophys. J. Int.*, *146*, 731–746, doi:10.1046/j.0956-540x.2001.01485.x.

Godfrey, N. J., F. Davey, T. A. Stern, and D. Okaya (2001), Crustal structure and thermal anomalies of the Dunedin Region, South Island, New Zealand, *J. Geophys. Res.*, *106*(B12), 30,835–30,848, doi:10.1029/2000JB000006.

Henrys, S. A., D. J. Woodward, D. Okaya, and J. Yu (2004), Mapping the Moho beneath the Southern Alps continent-continent collision, New Zealand, using wide-angle reflections, *Geophys. Res. Lett.*, *31*, L17602, doi:10.1029/2004GL020561.

Kohler, M. D., and D. Eberhart-Phillips (2002), Three-dimensional lithospheric structure below the New Zealand Southern Alps, *J. Geophys. Res.*, *107*(B10), 2225, doi:10.1029/2001JB000182.

Langston, C. A. (1979), Structure under Mount Rainier, Washington, inferred from teleseismic body waves, *J. Geophys. Res.*, *84*(B9), 4749–4762, doi:10.1029/JB084iB09p04749.

Melhuish, A., W. S. Holbrook, F. Davey, D. A. Okaya, and T. Stern (2005), Crustal and upper mantle seismic structure of the Australian plate, South Island, New Zealand, *Tectonophysics*, *395*, 113–135, doi:10.1016/j.tecto.2004.09.005.

Mortimer, N., F. J. Davey, A. Melhuish, J. Yu, and N. J. Godfrey (2002), Geological interpretation of a deep seismic reflection profile across the Eastern Province and Median Batholith, New Zealand: Crustal architecture of an extended Phanerozoic convergent orogen, *N. Z. J. Geol. Geophys.*, *45*, 349–363.

Norris, R.J., P. Koons, and A.P. Cooper (1990), The obliquely-convergent plate boundary in the South Island of New Zealand, *J. Struct. Geol.*, *12*, 715–725, doi:10.1016/0191-8141(90)90084-C.

Owens, T. J., R. S. Crosson, and M. A. Hendrickson (1988), Constraints on the subduction geometry beneath western Washington from broadband teleseismic waveform modeling, *Bull. Seismol. Soc. Am.*, *78*(3), 1319–1334.

Parker, P. B. (1999), Genetic algorithms and their use in geophysical problems, Ph.D. thesis, 202 pp., Univ. of Calif., Berkeley.

Platt, J. P. (1993), Exhumation of high-pressure rocks: a review of concepts and processes, *Terra Nova*, *5*, 119–133, doi:10.1111/j.1365-3121.1993.tb00237.x.

Savage, M. K., J. Park, and H. Todd (2007), Velocity and anisotropy structure at the Hikurangi subduction margin, New Zealand from receiver functions, *Geophys. J. Int.*, *168*, 1034–1050, doi:10.1111/j.1365-246X.2006.03086.x.

Scherwath, M., T. Stern, F. Davey, D. Okaya, W. S. Holbrook, R. Davies, and S. Kleffmann (2003), Lithospheric structure across oblique continental collision in New Zealand from wide-angle *P* wave modeling, *J. Geophys. Res.*, *108*(B12), 2566, doi:10.1029/2002JB002286.

Sutherland, R. (1999), Basement geology and tectonic development of the greater New Zealand region: An interpretation from regional magnetic data, *Tectonophysics*, *308*, 341–362, doi:10.1016/S0040-1951(99)00108-0.

Sutherland, R., F. Davey, and J. Beavan (2000), Plate boundary deformation in South Island, New Zealand, is related to inherited lithospheric structure, *Earth Planet. Sci. Lett.*, *177*, 141–151, doi:10.1016/S0012-821X(00)00043-1.

Van Avendonk, H. J. A., W. S. Holbrook, D. Okaya, J. K. Austin, F. Davey, and T. Stern (2004), Continental crust under compression: A seismic refraction study of South Island Geophysical Transect I, South Island, New Zealand, *J. Geophys. Res.*, *109*, B06302, doi:10.1029/2003JB002790.

Walcott, R. I. (1998), Modes of oblique compression: Late Cenozoic tectonics of the South Island of New Zealand, *Rev. Geophys.*, *36*(1), 1–26, doi:10.1029/97RG03084.

Warner, M., J. Morgan, P. Barton, C. Price, and K. Jones (1996), Seismic reflections from the mantle represent relict subduction zones within the continental lithosphere, *Geology*, *24*, 39–42, doi:10.1130/0091-7613(1996)024<0039:SRFTMR>2.3.CO;2.

Woodward, D. J. (1979), The crustal structure of the Southern Alps, New Zealand, as determined by gravity, *Bull. R. Soc. N. Z.*, *18*, 13–20.

Zhu, L., and H. Kanamori (2000), Moho depth variation in Southern California from teleseismic receiver functions, *J. Geophys. Res.*, *105*(B2), 2969–2980, doi:10.1029/1999JB900322.

R. W. Clayton and S. Spasojević, Seismological Laboratory, California Institute of Technology, 1200 E. California Blvd., Pasadena, CA 91125, USA. (clay@gps.caltech.edu; skisin@gps.caltech.edu)